SCIENTIFIC REPORTS

OPEN

SUBJECT AREAS:
FERROELECTRICS AND MULTIFERROICS
SPINTRONICS
ELECTRONIC STRUCTURE

Received
21 October 2013

Accepted
12 March 2014

Published
4 April 2014

Correspondence and requests for materials should be addressed to W.Y.Z. (wyzhang@nju.edu.cn)

First-principles study on the phase diagram and multiferroic properties of $(SrCoO_3)_1/(SrTiO_3)_1$ superlattices

Guang Song & Weiyi Zhang

National Laboratory of Solid State Microstructures and Department of Physics, Nanjing University, Nanjing 210093, China.

To design a multiferroic material at atomic scale, strong spin-lattice and charge-lattice couplings play crucial roles. Our first-principles calculation on $(SrCoO_3)_1/(SrTiO_3)_1$ superlattices, with above coupling properties, yields a rich physical phase diagram as a function of epitaxial strain. In particular, a robust ferroelectric ferromagnetic insulator of Pc symmetry is stabilized at tensile strain $\Delta a/a_0$ = 0.86%–5.53%. The polarization can be as large as 36 $\mu C/cm^2$ and magnetic moment can reach 6μ_B per unit cell. The magnetocrystalline anisotropy energy (0.16 meV/Co in (001) plane, 0.6 meV/Co in (100) plane) is comparable with that of $TbMnO_3$ compound and the magnetoelectric constant α (1.44×10^{-3} Gaussian unit) is comparable with that of $Co_3B_7O_{13}Br$ compound. Our study suggests that epitaxially strained $(SrCoO_3)_1/(SrTiO_3)_1$ superlattices not only offer an excellent candidate for multiferroic materials, but also demonstrate the half-metal and ferromagnetic insulator properties with potential application in spintronic devices.

A ferroelectric ferromagnetic insulator can be a good candidate for multiferroic materials if the cross control of polarization or magnetization by magnetic or electric field can be manipulated[1,2]. Thus, a satisfactory multiferroic compound not only possesses large polarization and magnetization, but also requires strong magnetoelectric coupling[3,4]. As device miniaturization demands integrating electronic and magnetic components together, searching for new multiferroic materials constitutes an important research direction[5,6].

The perovskite family of compounds offers an excellent candidate for multiferroic materials because of the strong coupling among spin, charge, and orbital degrees of freedom[7,8]. In particular, the subtle balance between different competing interactions makes the structural tuning very effective so that novel phenomena appear in the presence of either compressive or tensile strain[9–11]. Among others, Lee *et al.* demonstrated the feasibility of converting nonferroelectric and nonferromagnetic $EuTiO_3$ films into multiferroics under epitaxial tensile strain imposed by substrates[12,13]. The critical temperature T_C (=4.24 K) was very low, it, nevertheless, provided a new direction to explore multiferroic materials. The substrate induced strain also helps to make the $LuFeO_3$ thin films a room temperature multiferroic, a weak ferromagnetism was observed at 130 K resulting from spin reorientation phenomena[14]. Inspired by the experimental advances, the first-principles studies have also offered valuable information in this endeavor. The multiferroic property has been predicted by Lee *et al.* in $SrMnO_3$ thin films under epitaxial strain and T_C = 92 K was estimated[15]. An interesting phase transition between a ferromagnetic metal and ferroelectric antiferromagnetic (AFM) insulator is also shown in strained $SrCoO_3$ thin film[16]. There are also attempts to transform ferroelectric compounds into multiferroic compounds by doping. For instance, ferromagnetism was induced in V-doped ferroelectric $La_2Ti_2O_7$ compound[17], but the magnetoelectric coupling was too weak to function as a multiferroic. Although great processes have been made in the search of multiferroic materials, many important issues remain unresolved. The critical temperature is still low which hinders applications; compounds with both large polarization and magnetization are rare; even if large polarization and magnetization have been achieved, strong magnetoelectric coupling still needs to be dealt with.

Since epitaxial strain plays such an important role in tuning material properties, combining crystals with similar structures but complementary properties into superlattices can be a good option[18,19]. One expects that the resultant materials might combine the characteristics of their constituents. Furthermore, interface mediated strain effectively couples the physical properties of their constituents so that the cross controls of constituent properties can be realized. In the recent studies on superlattice structures, the improper ferroelectric effect was found in $PbTiO_3/SrTiO_3$ superlattices[18] and a large magnetoelectric coupling was also observed in nonferroelectric $NdMnO_3/SrMnO_3/LaMnO_3$ superlattices[19]. To shed further insight of interface effect on material

properties, we have studied, in this Report, the electronic and magnetic properties of $(SrCoO_3)_1/(SrTiO_3)_1$ superlattice (made of $SrCoO_3$ and $SrTiO_3$ layers of one cubic-cell thick, SCO/STO). As is well known, $SrCoO_3$ is a prototype spin-state transition compound[20] and possesses strong Jahn-Teller effect while $SrTiO_3$[11], though belongs to paraelectric compound, is near the ferroelectric instability. It is hoped that large ferroelectricity and ferromagnetism can arise from its constituent compounds while strong magnetoelectric coupling can be achieved by the interface mediated spin-lattice and charge-lattice couplings.

To explore the phase diagram of SCO/STO superlattices, possible crystal structures with different oxygen octahedra tilting (OOT) patterns are derived from the unstable phonon modes of high symmetry P4/mmm structure and their relative stabilities are analyzed. In Glazer's notation[21], the considered metastable crystal structures include: P4/mmm ($a^0a^0c^0$), P4mm (Γ_3^-), Amm2 (Γ_5^-), P4/mbm ($a^0a^0c^+$), C2/m ($a^-a^0c^0$), Pmna ($a^-a^-c^0$), P21/c ($a^-a^-c^+$), Pbam (P4/mbm with Jahn-Teller distortion), P4bm (P4/mbm + Γ_3^-), Cm (C2/m + Γ_3^-), Pma2 (Pmna + Γ_3^-), Pc (P21/c + Γ_3^- + Γ_5^-), and Pba2(Pbam + Γ_3^-) symmetries. Γ_3^- and Γ_5^- refer to the polar distortion modes perpendicular and parallel to the (001) plane of superlattices (see Supplementary Information). In addition, both ferromagnetic (FM) and nearest neighbor antiferromagnetic (AFM) states are considered for cobalt moments. Although the Co-ion is well known for its varying spin-state depending on crystal field, the intermediate spin-state turns out to be the convergent solution in the whole epitaxial strain range we studied. In our numerical calculations, for a given initial structure with characteristic OOT pattern and polar distortion, we search for the convergent metastable solution driven by the structural and atomic relaxations. The convergent solution can be either the one with the same symmetry as the initial trial solution or a solution with different symmetry.

Results

In Fig. 1, we plot the energies of those possible ground states for the strain range $e = -5.6\% \sim 5.89\%$. As strain varies from compression to tensile, the ground state of the superlattices changes consecutively from the antiferromagnetic metal of P4mm symmetry to the ferromagnetic half-metal, insulator, and again half-metal of Pbam symmetry, then to the ferromagnetic insulators with almost degenerate P21/c and C2/m symmetries, and is followed by the robust multiferroic insulator of Pc symmetry with large polarization and magnetization combined with strong magnetoelectric coupling. This state is finally replaced by the antiferromagnetic insulator of Pc structure. To correlate the electromagnetic properties of possible ground states with the specific crystal structures, the lattice constant c, OOT, band-gap, and exchange energy are presented in Fig. 2. AAFD of Fig. 2b stands for the anti-phase antiferro-distortive vector of OOT[22], its three components are the tilting angles along the pseudo-cubic crystal cell ([100], [010], and [001]). Since the AAFD vectors for CoO_6 and TiO_6 octahedra are complementary to each other, only AAFD vectors for CoO_6 octahedra are shown.

Below we discuss the electronic and magnetic properties of various possible ground states one by one. For $-5.6\% < e \leq -4.3\%$, the most stable state is an AFM metal with P4mm symmetry (see Supplementary Information). This state has no OOT and the band gaps for both spin-up and spin-down bands are zero. The projected electron occupation number and magnetic moment on Co-d orbitals are $n_d^{Co} \approx 6.86$ and $m_d^{Co} \approx 2.75\mu_B$. The Co ions take an intermediate-spin state and form an AFM order.

As strain e approaches -4.3%, above AFM state is replaced by a ferromagnetic state with Pbam symmetry. From the band-gap shown in Fig. 2c, this state is initially a half metal with perfect spin polarization. The half-metal state is further developed into a ferromagnetic insulator at $e = -3.45\%$. The band-gaps for both spin-up and spin-down bands become nonzero though one decreases while another increases with epitaxial strain e. A half-metal state with reversed spin polarization could be recovered at $e = -0.01\%$ which is, however, beyond the border ($e = -0.57\%$) of stability for this

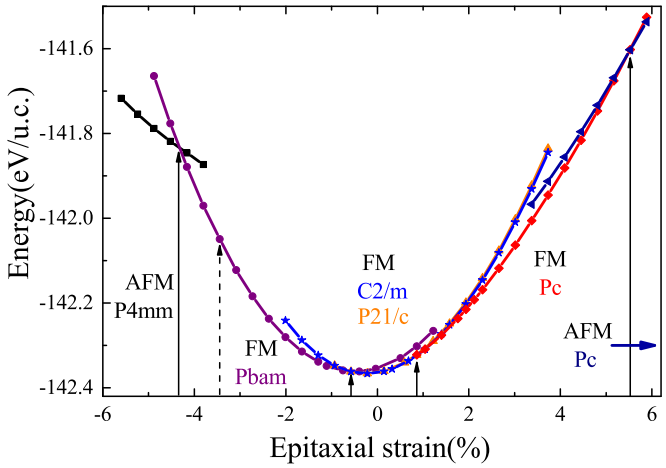

Figure 1 | Energies of SCO/STO superlattices as functions of epitaxial strain *e* for the various possible ground states of different symmetries. $e = (a - a_0)/a_0$ is defined with respect to the equilibrium lattice constant $a_0 = 3.940$Å of $SrTiO_3$. The vertical lines mark the phase boundaries between different symmetries while the dotted vertical line represents the metal-insulator boundary within the same structural symmetry.

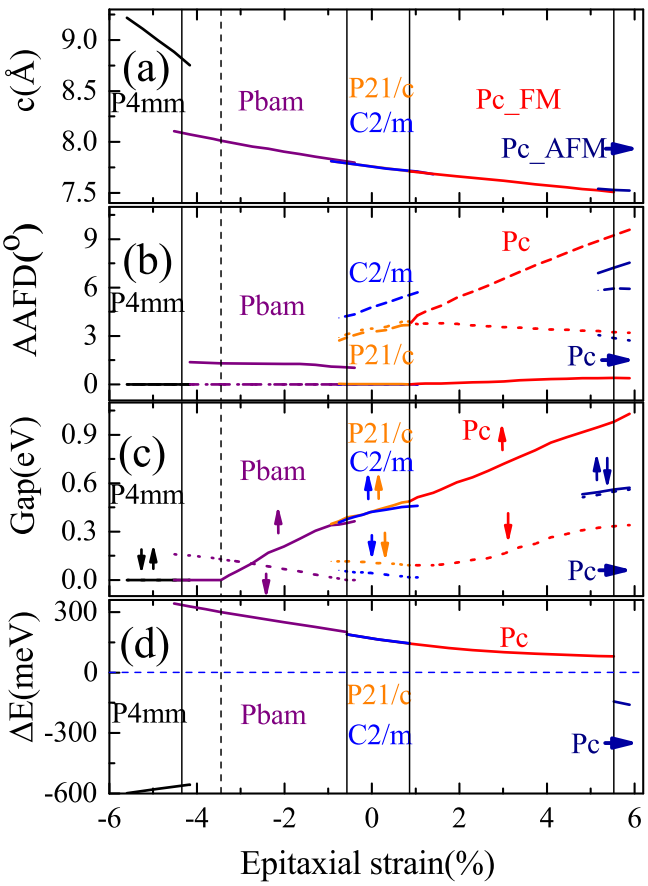

Figure 2 | Structural and electronic properties of SCO/STO superlattices versus epitaxial strain for the various possible ground states. (a) Lattice constant c; (b) AAFD vector. Dashed, dotted, and solid lines represent x, y, z components, respectively; (c) Band gaps. Solid and dotted lines refer to spin-up and spin-down bands; (d) Exchange energy $\Delta E = E_{AFM} - E_{FM}$.

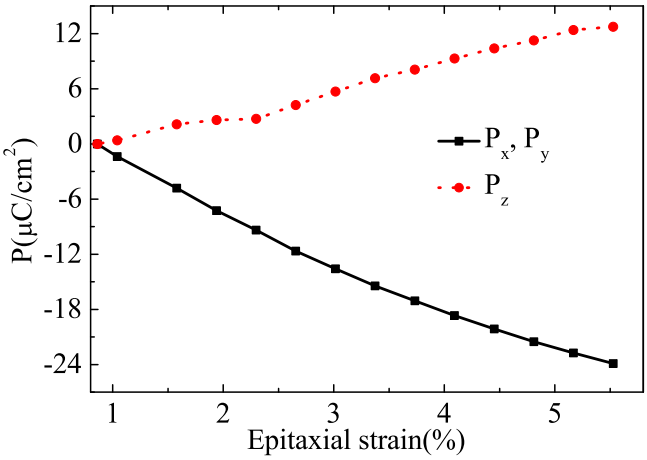

Figure 3 | The polarization of the robust multiferroic state of Pc structure as a function of tensile strain.

state. AAFD vector changes very slowly with epitaxial strain, the only nonzero titling angle along z-axis changes from 1.38° to 1.02° in the strain range (−4.3%, −0.57%). The electron occupation number ($n_d^{Co}\approx6.90$) is almost unchanged while magnetic moment ($m_d^{Co}\approx2.25\mu_B$) is reduced. These half-metal and ferromagnetic insulator may find their applications in spintronic devices[23].

In the region $-0.57\% < e \leq 0.86\%$ where strain is small, the two ferromagnetic insulators with separate P21/c and C2/m symmetries appear as the most stable states. These two states are almost degenerate in energy and their crystal structures are all of monoclinic crystal class. Similar case was also found previously in $EuTiO_3$[24]. The lattice constants and exchange energies have similar values. The electron occupation numbers and magnetic moments are almost identical, $n_d^{Co}\approx6.90, m_d^{Co}\approx2.26\mu_B$ for both states. The band-gaps for spin-up bands are of the same sizes while the band-gaps for spin-down differ by a factor of two. This is caused by the different crystal structures. For P21/c structure, AAFD vector changes from (2.90°, 3.10°, 0.02°) to (3.68°, 3.89°, 0°). The x and y components are quite close, though not identical due to the orbital ordering similar to that in $LaMnO_3$[23]. For C2/m structure, only x component of AAFD vector is nonzero and takes the value 4.17° ~ 5.39° in the corresponding strain range.

At tensile strain $e = 0.86\%$, both energies and first derivatives of energies with respect to strain e are identical for P21/c and Pc structures. Thus, a second order phase transition takes place from P21/c to Pc structure. These two states are quite similar magnetically except the polar distortion in Pc structure. The ferromagnetic insulator is still kept in Pc structure and the band-gaps evolve continuously upwards with e. In the strain range (0.86%, 5.53%) stable for Pc structure, the AAFD vector varies from (3.68°, 3.89°, 0.00°) to (9.23°, 3.23°, 0.39°). The electron occupation number and magnetic moment are almost the same as those of P21/c structure. The total magnetic moment is $6\mu_B$. The most striking feature of this state is the large polarization as shown in Fig. 3. The calculated polarization with respect to P21/c reference structure lies along [uuv] direction with $u \neq v$. It increases linearly from (0, 0, 0) to (−23.9 μC/cm², −23.9 μC/cm², 12.75 μC/cm²) with the inclination angle of about 27°. This robust multiferroic state is a proper multiferroic state similar to the $Pmc2_1$ state found by Lee *et al.*[15]. It differs from the multiferroic states studied by other groups where only weak ferromagnetism or antiferromagnetism is found to coexist with ferroelectric order[14,25,26].

Further increasing the tensile strain destabilizes the ferromagnetic state and the AFM insulator of Pc structure becomes stable for $e >$ 5.53%. The x and y components of the AAFD vector are reduced significantly while the z component increases considerably. In comparison with the FM state of Pc structure, this state has the similar electron occupation number $\left(n_d^{Co}\approx6.91\right)$ and slightly reduced magnetic moment $\left(m_d^{Co}\approx2.11\mu_B\right)$. This state is also a multiferroic state, the calculated polarization is (27.9 μC/cm², 34.0 μC/cm², 32.9 μC/cm²) at $e = 5.89\%$.

To shed further insight into the physical properties of the multiferroic state of Pc structure, the spin and orbital resolved partial densities of states (PDOS) are presented in Fig. 4. The epitaxial strain is set at $e = 2.3\%$ and Fermi energy is set as zero. The Co-d orbitals are decomposed into triplet $t_{2g}(d_{xy}, d_{yz}, d_{zx})$ and doublet $e_g\left(d_{x^2-y^2}, d_{3z^2-r^2}\right)$ sets with respect to CoO_6 octahedron. The two nearest neighbors Co-I and Co-II ions are included in order to illustrate charge and orbital ordering phenomena. It is seen that the multiferroic state is an insulator with a band-gap of 0.12 eV.

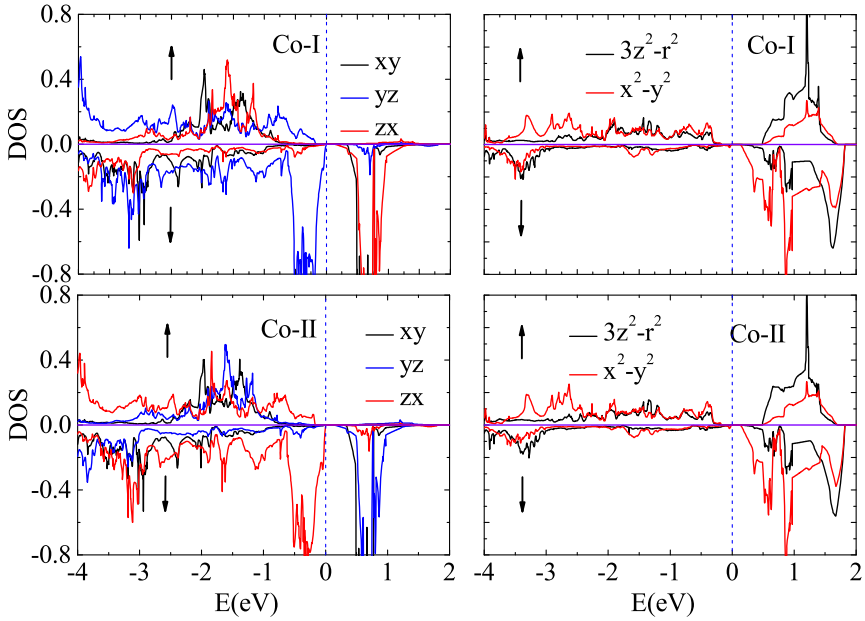

Figure 4 | The spin and orbital resolved partial densities of states of SCO/STO superlattices at $e = 2.3\%$. The spin-up PDOSs are plotted upwards while spin-down PDOS are plotted downwards. Other notations are described in the text.

PDOSs are the same for the d_{e_g}-orbitals of both Co-ions while those of $d_{t_{2g}}$-orbitals are almost the same if x and y-axes are interchanged for two Co-ions. To analyze the spin and orbital configurations, the projected electron occupation numbers are calculated for Co-ions within the muffin-tin radius of 1.25Å. For $d_{t_{2g}}$-orbitals, all spin-up states are almost occupied while only one of the spin-down states is occupied for each Co-type. The doubly occupied $d_{t_{2g}}$-orbital is d_{zx} for Co-I and d_{yz} for Co-II. Thus, the Co-ions form an antiferro-orbital ordering and take an intermediate spin state. Such orbital ordering is made possible by the spontaneous Jahn-Teller distortion similar to $LaMnO_3$[23] (see Supplementary Information). The periodic elongation of CoO_6 octahedra along x and y-axes is not only responsible for alternately doubly occupied d_{zx} and d_{yz}-orbitals, but also responsible for the different tilting angles along x and y-axes. We would like to emphasize that the Jahn-Teller distortion induced orbital-ordering is a typical feature for all the ground states of SCO/STO superlattices.

So far, we have obtained a ferroelectric ferromagnetic insulator with large polarization and magnetization. To verify whether such state is a genuine multiferroic state or not, the issues concerning the hysteresis loops for ferroelectricity and ferromagnetism as well as magnetoelectric coupling have to be addressed. While the hysteresis loop for ferroelectricity shows itself automatically by the double well structure, the hysteresis loop for the ferromagnetism has to be demonstrated through the magnetocrystalline anisotropy energy (MAE). By using the algorithms adopted by Xiang *et al.*[27], we compute the MAE of Co-ions of SCO/STO superlattice and the results are presented in Fig. 5a–b. The magnetic anisotropy energies are 0.16 and 0.61 meV at $e = 2.3\%$ in the (001) and (100) planes, respectively, which have the same order of magnitude as those of Mn-ions in the good multiferroic compound $TbMnO_3$[27]. Because of the oxygen octahedral tilting, the minima of MAE in (001) plane are located at 35° with respect to a-axis. The minimum of MAE in (100) plane is slightly off the (001) plane and at 93° measuring from c-axis. These data are consistent with the AAFD vector shown in Fig. 2(b) where y component (3.65°) is very close to the easy axis. Magnetoelectric constant can be similarly estimated using the technique devised by Íñiguez[28]. The dependences of polarization and magnetization as functions of polar-mode distortion are shown in Fig. 5c–d. The polar-mode is chosen as a linear interpolation between the paraelectric P21/c structure and the ferroelectric Pc structure[17]. The dielectric polarity $p_n^d = 55.9|q|$ (q is electron charge) and the magnetic analogue of the dielectric polarity $p_n^m = 27.64 \times 10^{-2}$ μ_B/Å can be extracted from the linear part of P and M. The corresponding eigenvalue $C_n = 15.07$ eV/Å^2 is obtained from the total energy shown in Fig. 1, and the volume of unit cell is 248.53Å^3. The estimated value of magnetoelectric constant is $\alpha = 1.44 \times 10^{-3}$ in Gaussian unit, which is comparable to that of $Co_3B_7O_{13}Br$[29]. To have a reliable magnetoelectric constant, as usual, a high convergence criterion (10^{-8} eV) is imposed throughout the computations. Thus, the tensile strained SCO/STO superlattices do show excellent multiferroic property with large polarization and magnetization as well as strong magnetoelectric coupling.

Discussion

The robustness of the multiferroic state is checked against the different exchange-correlation functionals and different values of Coulomb repulsion U. As shown in the phase diagram for LDA + U with $U_{eff} = 3.9$eV and GGA + U with $U_{eff} = 2.9$eV (see Supplementary Information), the strain values for transition points in Fig. 1 may shift somewhat, but the ordering of various ground states are never altered. Thus the overall shape of the phase diagram is independent of the specific exchange-correlation functionals and the specific value of U.

The physical mechanism underlying the multiferroic property of SCO/STO superlattices can be understood from the crystal structure and electron orbital occupation information (see Supplementary Information). The asymmetrical bond lengths around Co- and Ti-ions in the Pc structure demonstrate off-center polar distortion within the CoO_6 and TiO_6 octahedra. Thus, the electric polarization is contributed by both Co- and Ti-ions. The magnetism comes from the unpaired Co-d electrons. Since Co-ions are responsible for both electric polarization and magnetization, strong magnetoelectric coupling is, of course, expected. With regard to the origin of ferromagnetism in the Pc structure, to the zeroth order, the spin-up states of Co-ions are all occupied while only one of the spin-down states is occupied. The electron occupation is 6 electrons. If we switch to hole picture, the level scheme for holes is just the reverse of level scheme for electrons. In the hole picture, lowest two Co-d_{e_g}-orbitals and

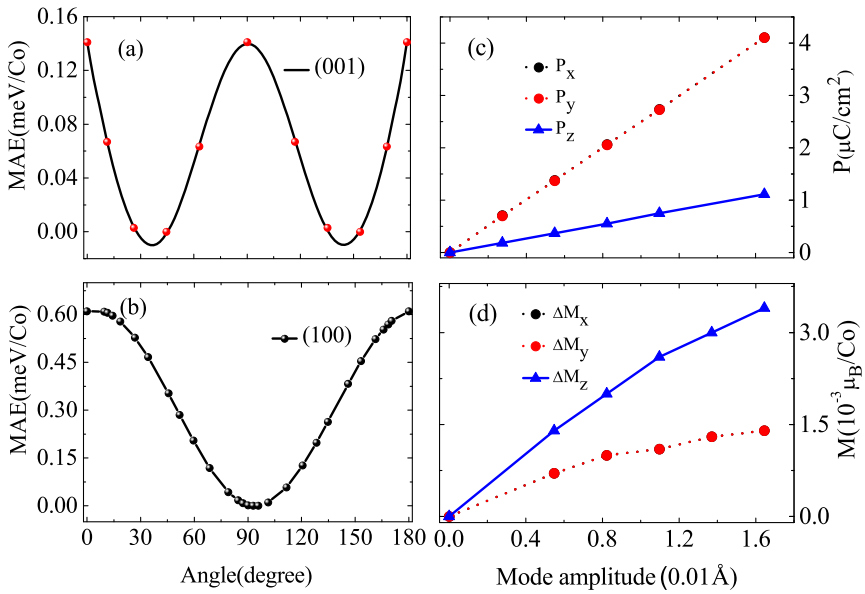

Figure 5 | The magnetocrystalline anisotropy energy, polarization, and magnetization. (a)–(b) MAE of Co-ions in the (001) and (100) planes, respectively; (c)–(d) polar-mode distortion dependence of polarization and magnetization. Solid lines refers to P_z, M_z, dotted lines to $P_x = P_y$, $\Delta M_x = \Delta M_y$. Other parameters are described in the text.

Co-$d_{t_{2g}}$-(xy)-orbital are singly occupied by spin-up holes. The nearest neighbor Co-$d_{t_{2g}}$-(yz) and $d_{t_{2g}}$-(zx) orbitals are alternatively occupied by a spin-up hole due to antiphase antiferrodistortive tilting of oxygen octahetra. The scenario here is quite similar to $LaMnO_3$ case except the exchange of electrons for holes. AFM state would be favored if the hole occupation is exactly four. Since the exact electron occupation number is large than 6, CoO_2 plane is intrinsically electron doped which favors the FM state according to the double exchange mechanism.

We have also extended our study to the generalized $(SrCoO_3)_n/(SrTiO_3)_m$ superlattices (n = 1,2,m = 1,2). The numerical analysis suggests that extended superlattice structures do not improve the material properties as a candidate for multiferroic compound. A close proximity between the ferromagnetic $SrCoO_3$ atomic layer and near ferroelectric $SrTiO_3$ atomic layer is the best configuration ensuring the novel multiferroic property. Deviating from this setting will either destabilize the ferromagnetism or favor metallic ground state.

In summary, comprehensive first-principles calculations have been carried out for the electronic and magnetic structures of SCO/STO superlattices and complex phase diagram has been obtained as a function of epitaxial strain. Half-metal and ferromagnetic insulator were discovered in the Pbam structure under compressive strain while a robust multiferroic state was found in tensile strained Pc structure. This ferroelectric ferromagnetic insulator has large polarization and magnetization, and strong magnetoelectric coupling arises from the strong piezoelectric and piezomagnetic coefficients as well as the peculiar orbital ordered structure. The calculated magnetocrystalline anisotropy energy is comparable to that of $TbMnO_3$ while the estimated interface mediated magnetoelectric coupling is comparable to that of $Co_3B_7O_{13}Br$. This robust multiferroic state offers an interesting alternative worthy of further experimental investigations.

Methods

Details of numerical computation. In this Report, the electronic structures were studied using a plane wave pseudopotential approach to the density-functional theory[30] as implemented in the Vienna *ab Initio* Simulation Package (VASP)[31]. We adopt the generalized gradient approximation with Perdew-Burke-Ernzerhof parametrization[32] and the Dudarev implementation[33] for the on-site Coulomb repulsion U and exchange interaction J_H. The projector augmented wave potentials[34] explicitly include 10 valence electrons for Sr ($4s^24p^65s^2$), 9 for Co ($3d^84s^1$), 12 for Ti ($3s^23p^64s^23d^2$), and 6 for O ($2s^22p^4$). The wave functions are expanded in a plane-waves basis with an energy cutoff of 600 eV. A $5 \times 5 \times 5$ Monkhorst-Pack k-point sampling is used for a $\sqrt{2} \times \sqrt{2} \times 1$ (20 atoms) unit cell. Each self-consistent electronic calculation is converged to 10^{-6} eV and the tolerance force is set to 0.005 eV/Å for the ionic relaxation. For Co 3d electrons, U_{eff} = 1.9eV reproduced the ferromagnetic structure with the correct lattice constant (a = 3.842Å) and magnetic moment ($2.967\mu_B$) for cubic $SrCoO_3$. This is in agreement with previous theoretical calculations[20] and experiment measurements[35,36]. For cubic $SrTiO_3$, a band insulator with the right lattice constant a = 3.940Å is also reproduced. To simulate an epitaxial strain, the in-plane lattice constant (a = b) of a $\sqrt{2} \times \sqrt{2} \times 1$ unit cell is fixed while the out-of-plane (c) lattice constant and atomic positions are allowed to relax. The ferroelectric polarization is computed using the Berry-phase approach[37].

1. Kimura, T. *et al.* Magnetic control of ferroelectric polarization. *Nature (London)* **426**, 55–58 (2003).
2. Hur, N. *et al.* Electric polarization reversal and memory in a multiferroic material induced by magnetic fields. *Nature (London)* **429**, 392–395 (2004).
3. Eerenstein, W., Mathur, N. D. & Scott, J. F. Multiferroic and magnetoelectric materials. *Nature (London)* **442**, 759–765 (2006).
4. Cheong, S.-W. & Mostovoy, M. Multiferroics: a magnetic twist for ferroelectricity. *Nature Mater.* **6**, 13–20 (2007).
5. Khomskii, D. Classifying multiferroics: Mechanisms and effects. *Physics* **2**, 20 (2009).
6. Heron, J. T. *et al.* Electric-field-induced magnetization reversal in a ferromagnet-multiferroic heterostructure. *Phys. Rev. Lett.* **107**, 217202 (2011).
7. Rondinelli, J. M. & Spaldin, N. A. Structure and properties of functional oxide thin films: Insights from electronic-structure calculations. *Adv. Mater.* **23**, 3363–3381 (2011).
8. Gupta, K., Mahadevan, P., Mavropoulos, P. & Ležaić, M. Orbital-ordering-induced ferroelectricity in $SrCrO_3$. *Phys. Rev. Lett.* **111**, 77601 (2013).
9. Diéguez, O., Rabe, K. M. & Vanderbilt, D. First-principles study of epitaxial strain in perovskites. *Phys. Rev. B* **72**, 144101 (2005).
10. Rata, A. D. *et al.* Strain-induced insulator state and giant gauge factor of $La_{0.7}Sr_{0.3}CoO_3$ films. *Phys. Rev. Lett.* **100**, 076401 (2008).
11. Zhang, J. Y. *et al.* Magnetism and local structure in low-dimensional Mott insulating $GdTiO_3$. *Phys. Rev. B* **88**, 121104(R) (2013).
12. Lee, J. H. *et al.* A strong ferroelectric ferromagnet created by means of spin–lattice coupling. *Nature (London)* **466**, 954–958 (2010).
13. Ke, X. & Freeland, J. W. Structural control of magnetic anisotropy in a strain driven multiferroic $EuTiO_3$ thin film. *Phys. Rev. B* **88**, 094434 (2013).
14. Wang, W. B. *et al.* Room-temperature multiferroic hexagonal $LuFeO_3$ films. *Phys. Rev. Lett.* **110**, 237601 (2013).
15. Lee, J. H. & Rabe, K. M. Epitaxial-strain-induced multiferroicity in $SrMnO_3$ from first-principles. *Phys. Rev. Lett.* **104**, 207204 (2010).
16. Lee, J. H. & Rabe, K. M. Coupled magnetic-ferroelectric metal-insulator transition in epitaxially strained $SrCoO_3$ from first-principles. *Phys. Rev. Lett.* **107**, 067601 (2011).
17. Scarrozza, M., Filippetti, A. & Fiorentini, V. Ferromagnetism and orbital order in a topological ferroelectric. *Phys. Rev. Lett.* **109**, 217202 (2012).
18. Bousquet, E. *et al.* Improper ferroelectricity in perovskite oxide artificial superlattices. *Nature (London)* **452**, 732–736 (2008).
19. Rogdakis, K. *et al.* Tunable ferroelectricity in artificial tri-layer superlattices comprised of non-ferroic components. *Nat. Commun.* **3**, 1064 (2012).
20. Zhuang, M., Zhang, W. Y., Hu, A. & Min, N. B. Possible magnetic ground state in the perovskite $SrCoO_3$. *Phys. Rev. B* **57**, 13655 (1998).
21. Glazer, A. The classification of tilted octahedra in perovskites. *Acta Crystallogr. Sect. B* **28**, 3384–3392 (1972).
22. Kornev, I. A. *et al.* Phase diagram of $Pb(Zr,Ti)O_3$ solid solutions from first-principles. *Phys. Rev. Lett.* **97**, 157601 (2006).
23. Salamon, M. B. & Jaime, M. The physics of manganites: Structure and transport. *Rev. Mod. Phys.* **73**, 583 (2001).
24. Yang, Y. R., Ren, W., Wang, D. W. & Bellaiche, L. Understanding and revisiting properties of $EuTiO_3$ bulk material and films from first-principles. *Phys. Rev. Lett.* **109**, 267602 (2012).
25. Yang, Y. R. *et al.* Revisiting properties of ferroelectric and multiferroic thin films under tensile strain from first-principles. *Phys. Rev. Lett.* **109**, 057602 (2012).
26. Arévalo-López, A. M. & Attfield, J. P. Weak ferromagnetism and domain effects in multiferroic $LiNbO_3$-type $MnTiO_3$-II. *Phys. Rev. B* **88**, 104416 (2013).
27. Xiang, H. J., Wei, S.-H., Whangbo, M.-H. & Da Silva, J. L. F. Spin-orbit coupling and ion displacements in multiferroic $TbMnO_3$. *Phys. Rev. Lett.* **101**, 037209 (2008).
28. Íñiguez, J. First-principles approach to lattice-mediated magnetoelectric effects. *Phys. Rev. Lett.* **101**, 117201 (2008).
29. Clin, M., Rivera, J.-P. & Schmid, H. Linear and quadratic magnetoelectric effect in boracite $Co_3B_7O_{13}Br$. *Ferroelectrics* **79**, 173–176 (1988).
30. Loschen, C., Carrasco, J., Neyman, K. M. & Illas, F. First-principles LDA + U and GGA + U study of cerium oxides: Dependence on the effective U parameter. *Phys. Rev. B* **75**, 035115 (2007).
31. Kresse, G. & Hafner, J. *Ab initio* molecular dynamics for liquid metals. *Phys. Rev. B* **47**, 558 (1993).
32. Perdew, J. P., Burke, K. & Ernzerhof, M. Generalized gradient approximation made simple. *Phys. Rev. Lett.* **77**, 3865 (1996).
33. Dudarev, S. L. *et al.* Electron-energy-loss spectra and the structural stability of nickel oxide: An LSDA + U study. *Phys. Rev. B* **57**, 1505 (1998).
34. Blöchl, P. E. Projector augmented-wave method. *Phys. Rev. B* **50**, 17953 (1994).
35. Taguchi, H., Shimada, M. & Koizumi, M. Magnetic properties in the system $La_{1-x}Sr_xCoO_3$ ($0.5 \leq x \leq 1.0$). *Mater. Res. Bull.* **13**, 1225–1230 (1978).
36. Long, Y. W. *et al.* Synthesis of cubic $SrCoO_3$ single crystal and its anisotropic magnetic and transport properties. *J. Phys. Condens. Matter.* **23**, 245601 (2011).
37. King-Smith, R. D. & Vanderbilt, D. Theory of polarization of crystalline solids. *Phys. Rev. B* **47**, 1651 (1993).

Acknowledgments

This work was supported in part by the National Basic Research Program of China (Grant No. 2010CB923404). We thank the High Performance Computing Center of Nanjing University for part of the numerical calculations.

Author contributions

W.Y.Z. supervised the work and G.S. carried out the numerical calculations of this work. G.S. and W.Y.Z. both contributed to the analysis and interpretation of results, and the writing of manuscript.

Additional information

Supplementary information accompanies this paper at http://www.nature.com/scientificreports

Competing financial interests: The authors declare no competing financial interests.

How to cite this article: Song, G. & Zhang, W.Y. First-principles study on the phase diagram and multiferroic properties of $(SrCoO_3)_1/(SrTiO_3)_1$ superlattices. *Sci. Rep.* **4**, 4564; DOI:10.1038/srep04564 (2014).